

Plasma rotation driven by static nonresonant magnetic fields^{a)}

A. M. Garofalo,^{1,b)} W. M. Solomon,² M. Lanctot,³ K. H. Burrell,¹ J. C. DeBoo,¹
J. S. deGrassie,¹ G. L. Jackson,¹ J.-K. Park,² H. Reimerdes,³ M. J. Schaffer,¹ and
E. J. Strait¹

¹General Atomics, P.O. Box 85608, San Diego, California 92186-5608, USA

²Princeton Plasma Physics Laboratory, P.O. Box 451, Princeton, New Jersey 08543-0451, USA

³Columbia University, 2960 Broadway, New York, New York 10027-1754, USA

(Received 19 December 2008; accepted 14 April 2009; published online 18 May 2009)

Recent experiments in high temperature DIII-D tokamak [J. L. Luxon, Nucl. Fusion **42**, 64 (2002)] plasmas reported the first observation of plasma acceleration driven by the application of static nonresonant magnetic fields (NRMFs), with resulting improvement in the global energy confinement time. Although the braking effect of static magnetic field asymmetries is well known, recent theory [A. J. Cole *et al.*, Phys. Rev. Lett. **99**, 065001 (2007)] predicts that in some circumstances they lead instead to an *increase* in rotation frequency toward a “neoclassical offset” rate in a direction opposed to the plasma current. We report the first experimental confirmation of this surprising result. The measured NRMF torque shows a strong dependence on both plasma density and temperature, above expectations from neoclassical theory. The consistency between theory and experiment improves with modifications to the expression of the NRMF torque accounting for a significant role of the plasma response to the external field and for the beta dependence of the plasma response, although some discrepancy remains. The magnitude and direction of the observed offset rotation associated with the NRMF torque are consistent with neoclassical theory predictions. The offset rotation rate is about 1% of the Alfvén frequency or more than double the rotation needed for stable operation at high β_N above the $n=1$ no-wall kink limit in DIII-D. © 2009 American Institute of Physics. [DOI: [10.1063/1.3129164](https://doi.org/10.1063/1.3129164)]

I. INTRODUCTION

An outstanding problem for a nuclear fusion reactor based on the tokamak confinement concept is that of imparting sufficient toroidal rotation to a high-density plasma. Toroidal rotation has been shown to be beneficial for a number of reasons, including the effect on energy confinement from toroidal rotation shear stabilization of turbulence,¹ and the yet not well-understood effect on the β threshold for stability of neoclassical tearing modes² [$\beta = \langle p \rangle / (B^2 / 2\mu_0)$ is the dimensionless plasma pressure and $\beta_N = \beta / (I_p / aB)$ is the normalized β , with I_p as the toroidal plasma current, a as the plasma minor radius, and B as the magnetic field strength]. Some minimum values of the toroidal rotation are even considered essential to avoid the problems of error field penetration, and at very high β_N (such as in an advanced tokamak reactor) to stabilize resistive wall modes.³ All of these rotation effects tend to improve the plasma performance or reduce the risk of disruptions.

The same tool that is used in many tokamak experiments to heat up a plasma, neutral beam injection (NBI), also imparts momentum to the plasma. However, a burning plasma does not need external sources of heat. On the other hand, a burning plasma does need to operate at high density to maximize the fusion triple product of plasma density, confinement time, and temperature. The penetration of neutral beams is strongly reduced with increasing plasma density, therefore

NBI for toroidal momentum injection becomes a very costly addition to a fusion reactor.

It has been observed that plasmas exhibit a nonzero toroidal rotation even in the absence of external momentum injection.^{4,5} A characteristic of this “intrinsic” rotation that is common to different tokamaks is that, when normalized to the ion thermal velocity, the intrinsic rotation at large minor radius increases with β_N . The direction of the intrinsic rotation is $\text{co-}I_p$ for discharges in a high-confinement mode (H -mode). Although this rotation may not be negligible in a fusion reactor, theories do not exist that can predict its characteristics.

While toroidal momentum sources are uncertain or expensive to come by, toroidal momentum sinks will be unavoidable in a fusion reactor. In addition to the angular momentum losses from turbulence and viscosity, unavoidable magnetic nonaxisymmetries (field errors) apply torques that can reduce the rotation. The physics of the interaction of nonaxisymmetric, static magnetic fields with a rotating plasma, has been the subject of extensive theoretical and experimental studies. It is useful to divide the nonaxisymmetric fields in two broad categories, depending on whether the structure of the magnetic field perturbation is resonant or nonresonant with respect to the field lines of the plasma. Without plasma rotation, resonant fields cause reconnection of the field lines close to the resonant surface, opening an island in the nested flux surface equilibrium topology. This effect is known to result in confinement degradation.⁶ Plasma rotation at a rate larger than the rate at which magnetic reconnection occurs leads to eddy currents on the resonant sur-

^{a)}Paper BI2 2, Bull. Am. Phys. Soc. **53**, 21 (2008).

^{b)}Invited speaker.

face that shield the plasma from the resonant error field. However, because of plasma resistivity, the shielding is not perfect and a braking torque inversely proportional to the plasma toroidal rotation results from the eddy currents crossed with the error magnetic field, $T_R \propto [(\tilde{B}_r/B)^2/V_\phi]$, where \tilde{B}_r/B is the perturbed radial field normalized to the equilibrium field and V_ϕ is the toroidal rotation velocity.⁷ Consistent with experimental observations, a simple “induction motor” model⁸ predicts a bifurcation of the plasma state, with a sudden loss of torque balance followed by reconnection, when the resonant field braking is large enough to reduce the rotation to half of the initial, no error-field level.

Nonresonant fields also can apply a braking torque on a rotating plasma, in general, proportional to the plasma rotation, $T_{NR} \propto (\tilde{B}_r/B)^2 V_\phi$. Although nonresonant fields cannot directly cause reconnection nor bifurcation, their braking torque can render the plasma less resilient to resonant error fields by reducing the threshold of the resonant error field above which a bifurcation occurs. Various processes contribute to the braking torque from nonresonant magnetic fields: untrapped-particle ripple drag, trapped-particle ripple drag, trapped-particle radial banana-drift effects. A simple model of the untrapped-particle ripple drag,⁹ related to “transit time magnetic pumping,” has been compared with various braking experiments conducted on the DIII-D tokamak using nonresonant fields of toroidal mode number $n=3$.^{10,11} In general, the torques predicted using vacuum calculations of the applied $n=3$ fields underestimate the measured torques, by as much as a factor of 5. More recently, a comparison of $n=3$ magnetic braking experiments on the National Spherical Torus Experiment¹² with theory, found better quantitative agreement by adding the calculations of untrapped-particle ripple drag and of trapped-particle radial banana-drift effects using a neoclassical toroidal flow damping model.^{13,14}

Predicting the effect of nonresonant fields on the plasma rotation has recently received increased attention because high- n fields (mostly nonresonant with respect to the plasma field lines, except for some resonant components near the plasma edge) have been shown to provide a tool to control the pressure gradients at the plasma edge, and ameliorate one of the major problems for tokamak-based approach to fusion, that is the large bursting instabilities called edge localized modes (ELMs).¹⁵ In a plasma with strong momentum injection from neutral beams, large amplitude high- n magnetic fields can be very beneficial by completely suppressing ELMs. On the other hand, in a reactor plasma with small external momentum injection, the braking torque from the nonresonant components of the high- n magnetic fields that are projected to be required for ELM suppression could lead to locked modes.

However, new work on the neoclassical theory of toroidal flows has highlighted a surprising feature implicit in the neoclassical theory,^{13,14} but not included in previous calculations:^{10–12} the prediction of a neoclassical “offset” rotation, V_ϕ^* , associated with the torque driven by static nonresonant magnetic fields (NRMFs), such that $T_{NRMF} \propto (V_\phi - V_\phi^*)$.¹⁶ This offset rotation is comparable in magnitude to the ion diamagnetic rotation, but it is in the counter- I_p

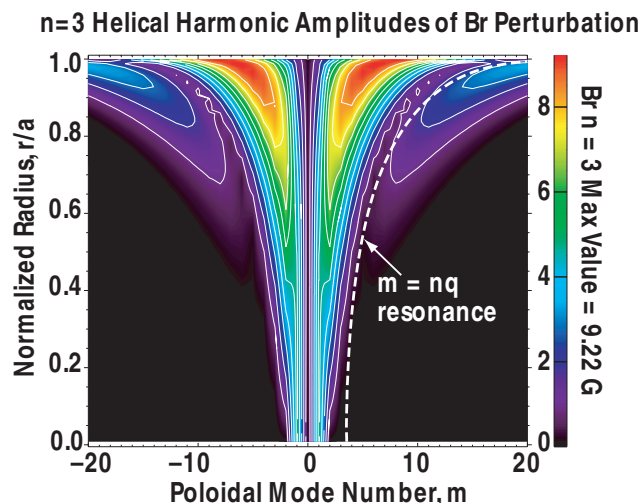


FIG. 1. (Color) Contour plot of the poloidal Fourier mode amplitudes for the $n=3$ field applied by the I-coil in the discharges considered in this paper, shown as a function of poloidal mode number m and normalized minor radius. The dashed line shows the loci of $m=nq$ resonance.

direction. In a plasma with near zero toroidal rotation, the application of nonresonant fields would lead to an acceleration toward the offset rotation value. In this case, the nonresonant torque acts in such a way to increase the resilience of the plasma to resonant error fields.

The first observation of plasma acceleration driven, in the counter- I_p direction, by the application of static NRMFs with resulting improvement in the global energy confinement time has been obtained in high temperature DIII-D tokamak plasmas.¹⁷ The next section of this paper, Sec. II, describes the discharge preparation and key equipment for these experiments. In Sec. III, the effect of the NRMF on plasma rotation and confinement is analyzed in detail, and in Sec. IV it is shown that the observed radial profile of the offset rotation is consistent with neoclassical theory predictions. The NRMF torque dependence on various plasma parameters in comparison with theoretical scalings and the importance of the plasma response to the external field are investigated in Sec. V. Section VI summarizes the results and discusses an important consequence: the large NRMF torque from high- n fields for ELM suppression in a fusion reactor may not represent a problem, but instead offer the potential that the plasma will rotate at a significant rate, a rate sufficient to provide confinement and stability benefits.

II. EXPERIMENTAL SETUP AND DISCHARGE PREPARATION

Nonresonant magnetic field perturbations are applied to DIII-D plasmas using the I-coil, a set of 12 picture-frame coils toroidally distributed at two poloidal locations: six above and six below the midplane.¹⁸ The high modularity of the I-coil provides the capability to apply $n=3$ fields that are almost purely non-resonant for the plasmas in this study, as illustrated in Fig. 1.

In the first set of experiments, the $n=3$ fields were applied to high β , high confinement (H -mode) plasmas with as close as possible the same cross-section shape, safety factor,

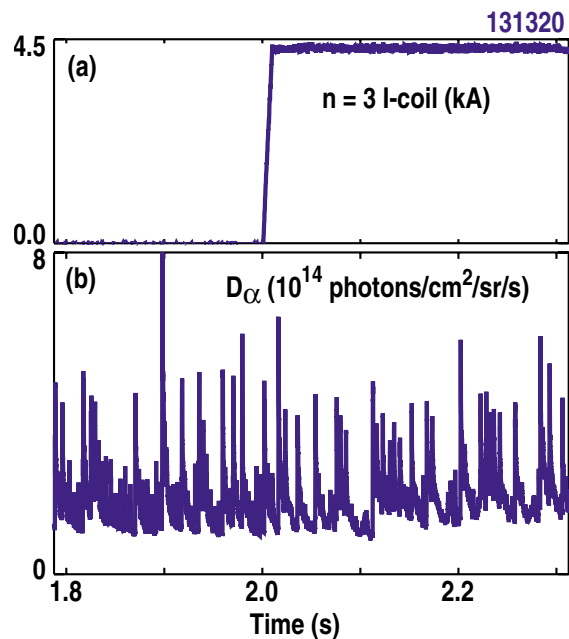


FIG. 2. (Color online) Time histories of (a) the I-coil current producing the $n=3$ field applied to the plasma and (b) the D_α light measured by a photodiode detector.

density, and temperature, but different toroidal rotation. The plasmas have a lower single null diverted cross section and monotonic safety-factor profile with value close to 1 on axis, and value at the 95% flux surface (q_{95}) of ~ 5.0 . These discharges were developed to isolate the effect of the $n=3$ field on rotation, therefore the q_{95} value was selected such that the applied $n=3$ fields are almost purely nonresonant with respect to the plasma field lines and have almost no effect on the ELM characteristics, as shown in Fig. 2.

Temperature, density, and the injected torque reach near stationary values before the $n=3$ field application. The density and injected torque are kept as much as possible constant across the time of field application. The density is controlled by simultaneous pumping and feedback-controlled gas puffing. The torque can be controlled by keeping the NBI power constant. However, in most cases part of the NBI power was feedback-controlled to keep constant the desired value of beta. In these cases, the NB actuators were chosen so that the net injected torque of the feedback controlled beams was zero (co- and counter- I_p directed beams).

A broad range of shot-to-shot NBI torque variation was achieved by matching plasma conditions with normal and reverse I_p direction, in addition to varying the mix of co- and counter- I_p NBIs. With the normal I_p direction, DIII-D offers the flexibility to choose the NB injectors among a pool of five co- I_p and two counter- I_p injectors. In addition, DIII-D offers the possibility to reverse the I_p direction. By matching plasma conditions with normal and reversed I_p direction, the plasma rotation was varied from the maximum (positive) value attained with ~ 4 co- I_p sources with normal I_p direction, to the minimum (negative) value attained with ~ 4 counter- I_p sources with reversed I_p direction (the desired high value of β required power from at least four NB injectors). The measured plasma rotation is the carbon impurity

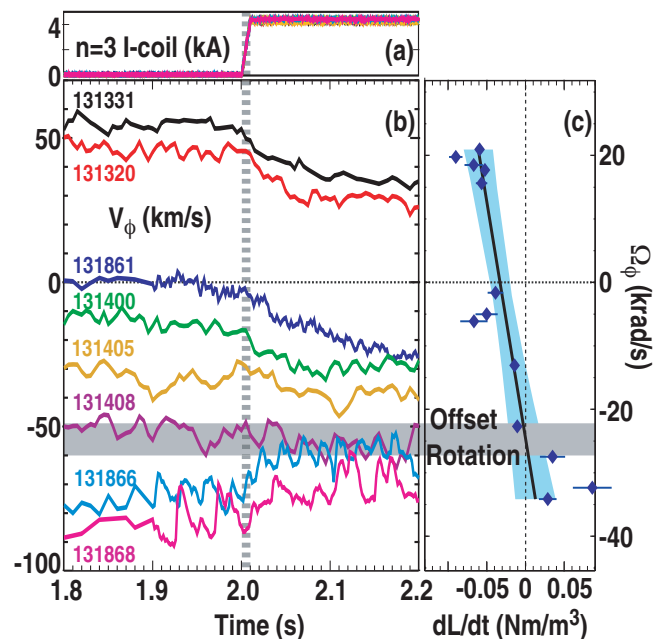


FIG. 3. (Color) Time histories of (a) amplitude of $n=3$ I-coil current and (b) toroidal rotation for plasmas with different values of the (constant) NBI torque (from -5.5 N m to 3.5 N m). (c) NRMF torque ($=dL/dt$) evaluated at the I-coil current turn-on time for a larger number of discharges. Note that the y-axis in (b) is rotation in km/s at fixed spatial CER view ($\rho \sim 0.8$, major radius $R \sim 2.2$ m), while in (c) it is rotation in krad/s at fixed ρ ($\rho = 0.8$). Nearly zero torque is measured for initial rotation approximately -50 km/s, indicating the offset rotation at $\rho \sim 0.8$.

ion rotation measured by charge exchange recombination spectroscopy (CER).

III. EFFECT OF NRMF TORQUE ON PLASMA ROTATION AND CONFINEMENT

Evidence of a counter- I_p offset rotation associated with the torque from a nonresonant magnetic field is shown in Fig. 3 by the results of the application of a large amplitude static $n=3$ field to similar discharges with different rotation values. In all cases the $n=3$ field is ramped, in 10 ms starting from $t=2$ s, up to the value corresponding to the maximum I-coil current ~ 4.4 kA $\pm 2\%$ [Fig. 3(a)]. All plasmas considered for this figure have β_N in the range $1.92 \pm 15\%$ and electron density n_e in the range $4.1 \times 10^{19} \text{ m}^{-3} \pm 5\%$. The discharges with near-zero or negative plasma rotation are obtained with reversed I_p . Figure 3(b) shows the plasma rotation measured at normalized minor radius $\rho \sim 0.8$ in the time range around the $n=3$ field turn on. When the $n=3$ field is eventually turned off, all discharges return to the rotation levels observed just before the $n=3$ field turn on, except occasional discharges which by then developed a locked $n=1$ tearing mode. The results of the $n=3$ field application are qualitatively similar for all minor radii. When the $n=3$ field is applied to a corotating plasma, a strong braking is observed. When the $n=3$ field is applied to a plasma with an already fast counter rotation, still a braking effect is observed, although somewhat smaller. When the $n=3$ field is applied to a near stationary or slowly counter-rotating plasma, a strong acceleration of the plasma rotation in the counter- I_p direction is observed. The accelera-

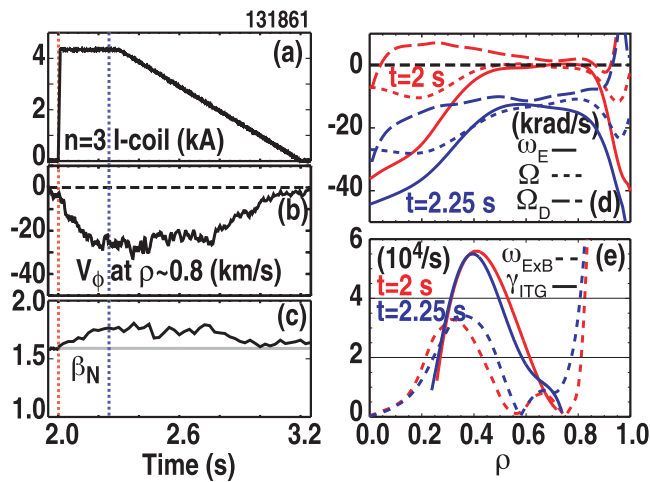


FIG. 4. (Color) Time histories of (a) $n=3$ I-coil current amplitude, (b) plasma toroidal rotation at $\rho \sim 0.8$, and (c) β_N (suppressed-zero y -axis) with constant injected power and momentum for a plasma (discharge 131861) with near-zero initial rotation at midradius. The vertical dashed lines in [(a)–(c)] indicate the times (color coded) for the radial profiles of (d) ω_E , the toroidal rotation of carbon (Ω) and deuterium (Ω_D), and of (e) the shearing rate ($\omega_{E \times B}$) and the calculated maximum growth rate for ion temperature gradient modes (γ_{ITG}).

tion cannot be explained by the applied $n=3$ field correcting an intrinsic $n=3$ error, since the same applied field causes braking on similar reversed- I_p plasmas with faster rotation. Furthermore, acceleration is also observed when applying an $n=3$ field with opposite toroidal phase. The results are consistent with neoclassical theory predicting a NRMF torque $T_{\text{NRMF}} \propto (V_\phi - V_\phi^*)$. At intermediate counter rotation the $n=3$ field has virtually no effect, yielding for the offset rotation at $\rho \sim 0.8$ a value $V_\phi^* \approx -50$ km/s.

The rotation change observed on a time scale of the angular momentum confinement time (~ 100 ms) from the $n=3$ field application is not a direct measure of the $n=3$ field torque, since changes in the energy and momentum confinement characteristics follow the changes in the rotation directly caused by the $n=3$ field torque. The local torque applied by the $n=3$ field has been measured by calculating the change in the time derivative of the angular momentum density, dL/dt , at the time the $n=3$ field is applied. To reduce the effect of unrelated fluctuations, the time derivative is calculated on a quadratic fit to the rotation data for times just following the $n=3$ field switch-on and on a linear fit to the nearly constant rotation for times just preceding the $n=3$ field turn-on and following the turn-off of the field. The measured local torque densities are shown in Fig. 3(c), together with a linear fit to the weighted measurements. Within the uncertainty in the measurements, the data are consistent with a behavior of the NRMF torque of the type $T_{\text{NRMF}} \propto (V_\phi - V_\phi^*)$.

The application of $n=3$ nonresonant fields to a plasma with near-zero or slow counter rotation produces an acceleration of the plasma rotation in the counter- I_p direction and an improvement of the global energy confinement time. This effect for one of the discharges (No. 131861) included in Fig. 3 is analyzed in detail in Fig. 4. The NBI power and torque are constant during the time range shown in the fig-

ure. The time history of the plasma rotation at $\rho \sim 0.8$ shows a large increase in rotation magnitude following the turn-on of the $n=3$ field. The rotation returns to pre- $n=3$ field levels as the nonaxisymmetric field is ramped back down to zero. The rotation acceleration happens at all minor radii, as shown in Fig. 4(d) by the radial profiles at times before and after the $n=3$ turn-on. The figure shows profiles of the measured rotation of carbon impurity ion and the rotation of the main ion species, deuterium. The deuterium rotation can be estimated neoclassically from the measured carbon rotation using the code NCLASS,¹⁹ which computes the poloidal rotation of a multispecies plasma in shaped geometry. In this way, the radial electric field E_r is computed for the impurity species using radial force balance and the deuterium rotation is solved under the assumption that all species experience the same E_r . However, it should also be noted that the difference between main ion and impurity rotation may not always be adequately described by neoclassical theory,^{20,21} although at least in these discharges there does not appear to be any significant discrepancy of the impurity carbon poloidal rotation compared with NCLASS predictions. The calculations show a strong increase in the main ion rotation following the application of the $n=3$ field. The time history of β_N shows an increase (over the unperturbed level) that correlates with the plasma rotation waveform. The increase in β_N at constant injected power is due to an improvement in the energy confinement. This confinement improvement (about 10%) is consistent with the paradigm of microturbulence stabilization by increased shear in the $E \times B$ flow.^{22,23} In a torus, the $E \times B$ shear stabilization criterion must be expressed in terms of the shear in the (species-independent) toroidal rotation driven by the radial electric field, $\omega_E = E_r / RB_\theta$.²⁴ Turbulence is affected when the shearing rate, $\omega_{E \times B} = [(RB_\theta)^2 / B] \times (\partial \omega_E / \partial \psi)$, becomes comparable to the linear growth rate of the turbulence. As shown in Fig. 4(d), ω_E increases significantly (in the counter direction) following the $n=3$ field application. The magnitude of the shearing rate, instead, shows only a slight increase for $0.3 < \rho < 0.6$, as indicated in Fig. 4(e). The figure also shows results from linear stability calculations with the TGLF code²⁵ predicting that, in the same core region, the maximum growth rate for ion temperature gradient modes is slightly reduced. The small increase in shearing rate and correspondent reduction in turbulence growth rate are consistent with the observed 10% improvement in energy confinement.

The observation that ω_E increases with the application of the $n=3$ field is particularly important. Not only is ω_E correlated with confinement improvement due to $E \times B$ shear stabilization of microturbulence; ω_E is also the key rotation parameter for macroscopic stability improvements. Recent high-beta experiments, which compared stability threshold rotation profiles in co- and counter-rotating plasmas, show that ω_E is the important rotation in the wall-stabilized regime (beta above the $n=1$ no-wall kink limit).²⁶ The neoclassical offset rotation of 50 km/s shown in this paper is about 1% of the Alfvén frequency and it is two to three times higher than the rotation needed for stable high beta operation in DIII-D.

IV. ANALYSIS OF THE OFFSET ROTATION

Neoclassical theory has long been used to understand the effects of nonresonant magnetic fields applied to an axisymmetric toroidal plasma.²⁷ Since the NRMF produces “ripples” in the magnetic field strength, particles can be trapped in new magnetic wells, and orbits of banana-trapped particles can be significantly modified. Both effects cause increased collisional transport, with an enhancement of the diffusion rate that is greater for the ions than for the electrons. This leads to nonambipolar radial ion particle fluxes and, in steady state, to radial currents that are necessary to maintain plasma charge neutrality. A toroidal torque on the bulk plasma ensues from the cross product of these “return” currents with the equilibrium poloidal magnetic field.

In the limit of very low ion collisionality ($\nu_i \sim 0$), the transport enhancement and therefore the NRMF torque, are predicted to increase with ν_i . This is the so-called ν -regime. At higher collisionality, another regime can be distinguished in the limit of the effective collisionality (the trapped-untrapped ion collision rate $\nu_{\text{eff}} = \nu_i / \varepsilon$, with ε as the plasma inverse aspect ratio) being much larger than the toroidal drift rate of the banana orbits (which is approximately the toroidal component of the $E \times B$ drift, $\omega_E = E_r / RB_\theta$), but smaller than $\omega_{ti} \sqrt{\varepsilon}$ (where $\omega_{ti} = \sqrt{T_i / m_i} / R_0 q$ is the ion transit frequency). At this higher collisionality, trapped particle effects (and therefore the transport enhancement and NRMF torque) diminish with increasing ν_i . This is the so-called $1/\nu$ -regime. The experimental data discussed in this paper fall between the ν and $1/\nu$ asymptotic limits.

It was only in the recent theoretical work by Cole *et al.*²⁸ that the existence of an “offset” rotation, such that $T_{\text{NRMF}} \propto (V_\phi - V_\phi^*)$, was pointed out explicitly. This offset rotation, which is comparable in magnitude to the ion diamagnetic frequency, but has direction opposed to the plasma current, can be written as

$$V_\phi^* = \frac{k_c}{Z_i e B_\theta} \frac{dT_i}{dr}, \quad (1)$$

with k_c depending on the collisionality regime. In the ν -regime limit it is $k_c \approx 0.9$. In the $1/\nu$ -regime limit is $k_c \approx 3.5$. A detailed model is still being developed in-between these limits, where the experimental data is situated.

The magnitude and radial dependence of the offset rotation observed in DIII-D has been compared to the theoretical scaling for the ν and $1/\nu$ collisionality regimes and it is found in qualitative agreement. The experimentally determined radial profile of the offset rotation can be approximated by the actual plasma rotation for discharge 131408 (intermediate counter rotation in Fig. 3), for which at any minor radius the $n=3$ braking produces no distinct angular momentum change. For a closer match of the plasma rotation to the offset rotation, the profile $V_\phi^{*,\text{exp}}(\rho)$ is evaluated at $t=2.25$ s, or several momentum confinement times into the phase with maximum $n=3$ field amplitude. Since the theoretical formulation of the offset rotation deals with main ion rotation, the radial profile of the calculated deuterium rotation is used for the experimental offset rotation $V_\phi^{*,\text{exp}}(\rho)$. The comparison of $V_\phi^{*,\text{exp}}(\rho)$ to neoclassical theory is shown by

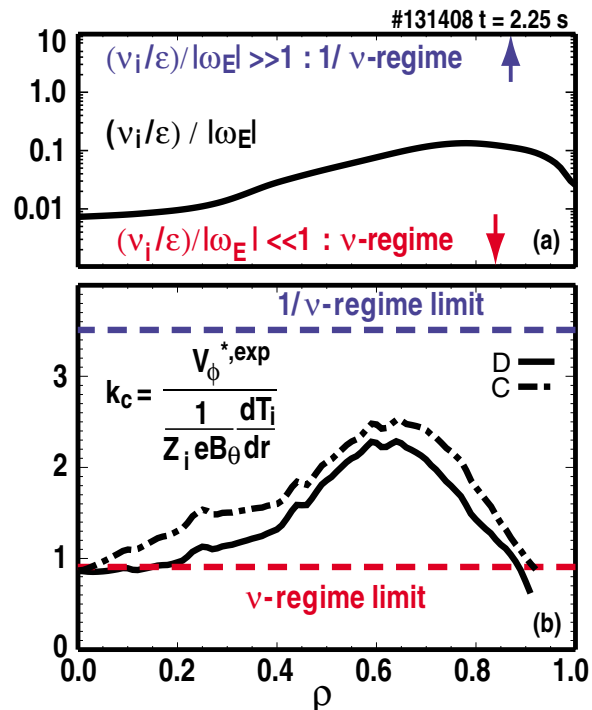


FIG. 5. (Color online) (a) Radial profile of $(\nu_i/\varepsilon)/|\omega_E|$ for discharge 131408 at $t=2.25$ s. (b) Radial profiles of k_c , indicating how the experimental offset rotation profile in the deuterium (solid line) and carbon (dot-dashed line) flow compares to the collisionality-dependent theoretical limits of the offset rotation.

the radial profile of $k_c = (V_\phi^{*,\text{exp}}) / [(1/Z_i e B_\theta)(dT_i/dr)]$ in Fig. 5(b). Figure 5(a) shows that at this time, the plasma is in the ν regime of collisionality to a varying degree for different values of ρ . The values of $k_c(\rho)$ fall between the theoretical limits for the ν and $1/\nu$ regimes. In particular, k_c is closer to the theoretical limit for the ν regime (~ 0.9) at the ρ values where the plasma is deeper in this regime, consistent with expectations. Given the uncertainties in the determination of the deuterium rotation, the profile of k_c obtained using the directly measured carbon rotation for $V_\phi^{*,\text{exp}}(\rho)$ is also shown for completeness. The results confirm that the experimental offset rotation is consistent with the semiquantitative neoclassical prediction. For a more detailed comparison between theory and experiment, a connecting formula between the two regimes is needed.

V. NRMF TORQUE VARIATION WITH PLASMA PARAMETERS

The rotation enhancement driven by nonresonant fields is strongly reduced at low β_N . Figure 6 illustrates the effect of the $n=3$ field on a pair of discharges with the same unperturbed rotation, but large difference in β_N . At higher β_N , a large acceleration is observed, while at lower β_N , little or no acceleration is seen.

At similar density, the β_N difference between these discharges is mostly due to a difference in the ion temperature. In the lower β_N discharge, both T_i and ∇T_i are reduced by about 40% in most of the plasma. Because of the low unperturbed rotation, the ∇T_i difference contributes almost a factor of ~ 2 to the reduced NRMF torque via a factor of ~ 2 re-

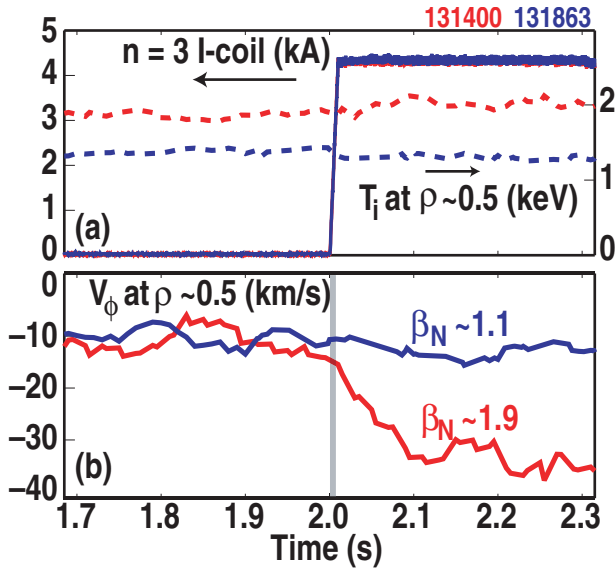


FIG. 6. (Color) Time histories of (a) $n=3$ I-coil current amplitude and ion temperature at midradius and (b) plasma toroidal rotation at midradius for two discharges with $\beta_N=1.1$ (131863, blue) and $\beta_N=1.9$ (131400, red), and same initial rotation.

duction in the offset rotation. To explain the approximate order of magnitude difference in the observed acceleration, a strong dependence of the NRMF torque on T_i must be invoked.

The dominant scaling factors in the neoclassical description of the NRMF torque depend on the collisionality regime. From Ref. 28, the NRMF torque for a plasma in the low collisionality ν -regime can be written as

$$T_{\text{NRMF},\nu} \propto \delta B^2 (V_\phi - V_\phi^*) n_i T_i^{-1/2} \omega_E^2, \quad (2)$$

while for a plasma in the higher collisionality $1/\nu$ regime, the NRMF torque can be written as

$$T_{\text{NRMF},1/\nu} \propto \delta B^2 (V_\phi - V_\phi^*) n_i^{-1} T_i^{5/2}, \quad (3)$$

where δB is the NRMF causing the torque and n_i is the ion density. Note that the dependence on δB and $(V_\phi - V_\phi^*)$ is identical for the two regimes, while the exponents are different for the dependencies on n_i , T_i , and ω_E .

The scalings of the NRMF torque observed in intermediate corotation DIII-D discharges have been compared to the theoretical scaling for the ν and $1/\nu$ collisionality regimes and it is found that the empirical scalings are not consistent with the predicted values for the two asymptotic limits, when only the I-coil is considered as source of the NRMF. The consistency improves when the contribution (estimated from modeling and measurements) of the plasma response to the total NRMF is included.

The first step in this analysis is to assume correct the theoretical scalings for δB and for $(V_\phi - V_\phi^*)$ in Eqs. (2) and (3). Later, these scalings will be tested together with the empirically determined scalings for the other parameters. At this stage, we neglect the plasma response, δB^{plasma} , to the $n=3$ I-coil field, δB^{ext} . Therefore the magnetic perturbation in the plasma is simply proportional to the $n=3$ I-coil current, δI_{ic} ,

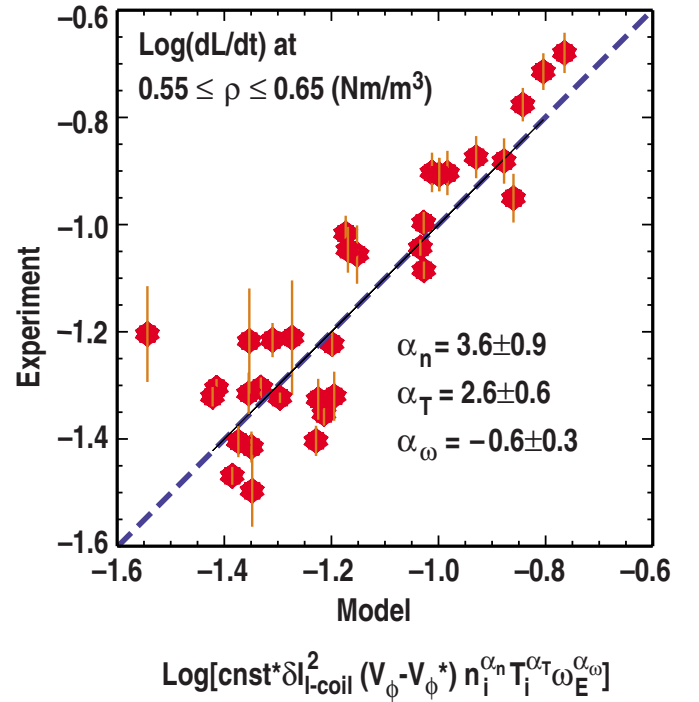


FIG. 7. (Color online) Multiple linear regression fit of the NRMF torque measurement logarithms for $0.55 \leq \rho \leq 0.65$ in a database of discharges with variation of the measured torque by up to a factor of 7. The coefficients determined by the fit are the exponents for n_i , T_i , and ω_E in the expression for the NRMF torque. Note that $n_i = n_e$ is assumed.

$$\delta B = \delta B^{\text{plasma}} + \delta B^{\text{ext}} \sim \delta B^{\text{ext}} \quad (4)$$

and

$$\delta B \propto \delta I_{\text{ic}}. \quad (5)$$

The scalings for n_i , T_i , and ω_E are determined from a multiple linear regression fit to the function

$$T_{\text{NRMF}} \propto \delta I_{\text{ic}}^2 (V_\phi - V_\phi^*) n_i^{\alpha_n} T_i^{\alpha_T} \omega_E^{\alpha_E} \quad (6)$$

of the NRMF torque measured in a group of discharges with $\pm 20\%$ variation in V_ϕ , $\pm 15\%$ variation in β_N , $\pm 25\%$ variation in n_i and T_i . The results are shown in Fig. 7 for the measurements at normalized minor radius $\rho=0.55-0.65$. This range of ρ is selected because the torque measurements have a larger variation (increasing the dynamic range in the regression) for $\rho < 0.7$, but are more accurate for $\rho > 0.5$.

TABLE I. Exponents of δI_{ic} , $(V_\phi - V_\phi^*)$, ω_E , n_i , and T_i in the theoretical expressions of the NRMF torque for the ν and $1/\nu$ collisionality regimes and exponents (bold) from the multiple linear regression fit of the experimental measurements to the NRMF torque function of Eq. (6). Exponents for δI_{ic} and $(V_\phi - V_\phi^*)$ are specified, since they are the same for the two collisionality regimes.

	ν	Experiment	$1/\nu$
δI_{ic}	2	2	2
$V_\phi - V_\phi^*$	1	1	1
ω_E	-2	-0.6 ± 0.3	0
n_i	1	3.6 ± 0.9	-1
T_i	-0.5	2.6 ± 0.6	2.5

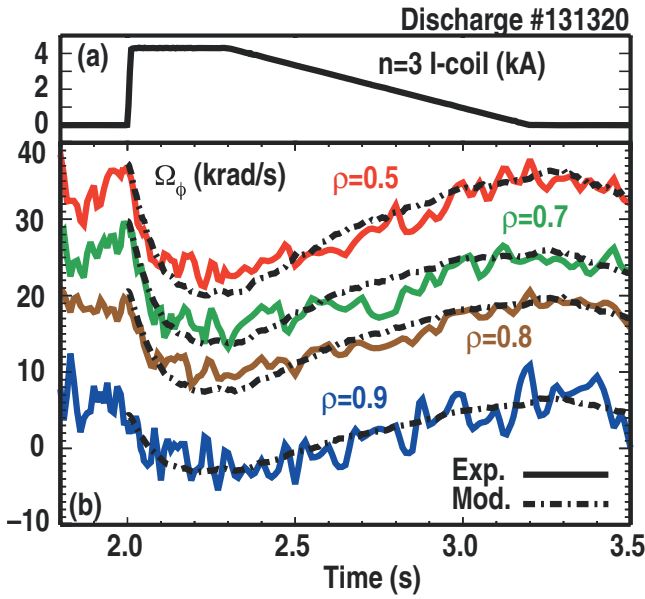


FIG. 8. (Color) Time histories of (a) the $n=3$ I-coil current and (b) the plasma toroidal rotation measured at various minor radial locations (solid lines). The dot-dashed lines are the plasma rotation evolution simulated using the TRANSP code.

The results of the multiple linear regression fit of the NRMF torque measurements show a strong dependence of the NRMF torque on the product $n_i T_i$, above the dependence expected from theory. The empirical scalings are compared to the theoretical scalings for the ν and $1/\nu$ regimes in Table I. Within the uncertainties, the exponents for T_i and ω_E fall between the two theoretical limits, but the exponent for n_i is clearly outside the range between the asymptotic limits.

In the above analysis of the NRMF torque scalings, the exponents for δB and $(V_\phi - V_\phi^*)$ in the theoretical expressions for the ν and $1/\nu$ collisionality limits are assumed adequate to represent the experimental data, since these exponents are identical for the two limits and the experimental data lies between those limits. In the next step of this analysis, these exponents are tested together with the empirically determined exponents for the other parameters: n_i , T_i , and ω_E .

In the test, illustrated in Fig. 8 (Ref. 29 for more details), the evolution of the plasma rotation profile measured in a discharge with strong NRMF braking is compared to the simulated evolution calculated using the momentum balance equation in TRANSP,³⁰

$$mnR \frac{\partial V_\phi}{\partial t} = \Sigma T + \nabla \cdot \left(mnR \chi_\phi \frac{\partial V_\phi}{\partial r} \right), \quad (7)$$

with prescribed NRMF torque and momentum diffusivity. The radial profile of the momentum diffusivity χ_ϕ is obtained from the rotation evolution observed without NRMF ($t < 2$ s and $t > 3.2$ s). The radial profile of the NRMF torque density is measured at $t=2$ s from the time rate of change of the angular momentum density, then evolved according to

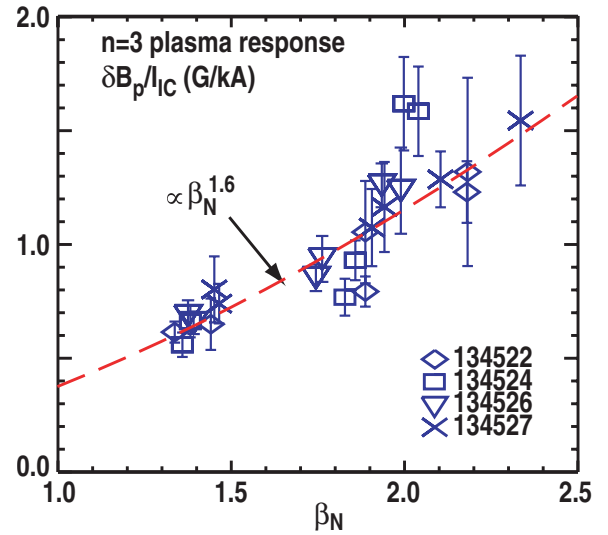


FIG. 9. (Color online) Magnetic measurements of the plasma response to the $n=3$ field applied by the I-coil normalized to the I-coil current versus the plasma β_N . Measured field is the perturbed poloidal magnetic field at the outboard midplane, just inside the vessel. Dashed line is the function $(\delta B_p^{\text{plasma}} / \delta I_{IC}) \propto \beta_N^{\alpha_\beta}$, which best fits the data ($\alpha_\beta = 1.6 \pm 0.2$).

$$T_{\text{NRMF}} \propto \delta I_{IC}^2 (V_\phi - V_\phi^*) n_i^{3.6} T_i^{2.6} \omega_E^{-0.6}. \quad (8)$$

The NBI torque is calculated with a Monte Carlo method using the experimental measurements at all times. The excellent agreement between measurements and simulations across the minor radius shows that the NRMF torque parameter dependence is indeed well described by the expression in Eq. (8) and that the effect of the $n=3$ I-coil field can be simply characterized by the application of a torque, without significant alterations to the momentum diffusivity profile.

Modifications to the torque function that explicitly account for the beta-dependent plasma response to the field applied by the I-coil can improve the consistency between the theoretical and empirical scalings for n_i and T_i . The $n=3$ plasma response is measured by an array of Mirnov sensors measuring the poloidal magnetic field at the outboard midplane, just inside the vessel. Because of the geometrical symmetry, these sensors have small coupling to the I-coils. Any residual coupling is removed in software, based on measurements without a plasma. Figure 9 shows that the $n=3$ magnetic field due to the plasma response is observed to increase with β_N . To characterize the β_N dependence with a simple relationship, valid at least in the small range $1.4 \leq \beta_N \leq 2.4$, we represent the measured normalized plasma response as $(\delta B_p^{\text{plasma}} / \delta I_{IC}) \propto \beta_N^{\alpha_\beta}$. Then, a linear regression fit of the logarithm of the measurements yields the exponent $\alpha_\beta = 1.6 \pm 0.2$.

Assuming that our external measurements of the plasma response give a representation of the behavior of the plasma response inside the plasma as well leads to rewriting the magnetic perturbation in the plasma [Eq. (5)] as

$$\delta B = \delta B^{\text{plasma}} + \delta B^{\text{ext}} \propto \delta I_{IC} \left[\left(\frac{\beta_N}{\beta_{N,0}} \right)^{1.6 \pm 0.2} + 1 \right], \quad (9)$$

where $\beta_{N,0}$ is the value of β_N at which the magnitudes of the plasma response and the $n=3$ I-coil field are comparable in the plasma.

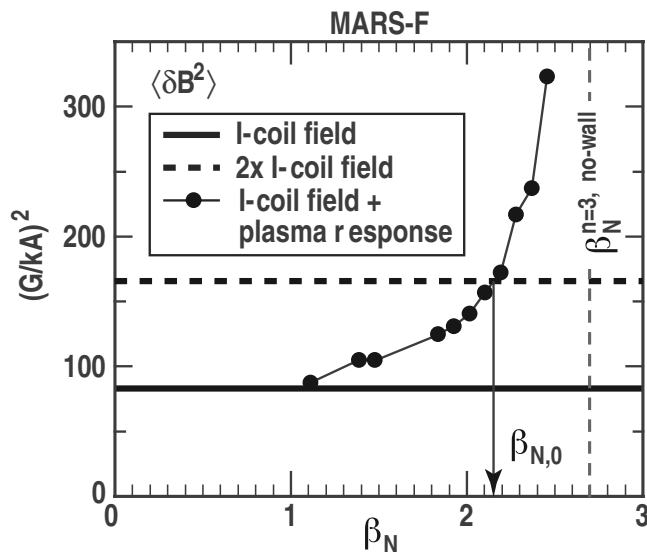


FIG. 10. MARS-F modeling of the beta dependence of the plasma response to the $n=3$ magnetic perturbation from the I-coil, based on equilibrium reconstruction of discharge No. 131321. Interpolated data points are the volume average of the total perturbed magnetic field inside the plasma, $\langle \delta B^2 \rangle = \langle \delta B_{\text{plasma}}^2 + \delta B_{\text{ext}}^2 \rangle$. Horizontal solid line is the volume average of the external field only, $\langle \delta B_{\text{ext}}^2 \rangle$. Horizontal dashed line is twice the value of $\langle \delta B_{\text{ext}}^2 \rangle$, therefore the intersection with the data interpolation yields $\beta_{N,0}$, i.e., the β_N value where $\langle \delta B_{\text{ext}}^2 \rangle \approx \langle \delta B_{\text{plasma}}^2 \rangle$. Vertical dashed line is the β_N stability limit for the $n=3$ kink without conducting wall.

An estimate of $\beta_{N,0}$ is obtained using the MARS-F code³¹ to model the ideal MHD plasma response to the $n=3$ I-coil field in presence of a resistive wall. The total perturbed magnetic field is calculated for a series of equilibria generated by scaling up and down the experimental pressure profile at fixed boundary and q -profile, starting from the equilibrium reconstruction of one of the discharges in the database of Fig. 7. From the results shown in Fig. 10, the value of β_N at which the volume averaged I-coil field and plasma response are comparable is $\beta_{N,0} \approx 2.15$. Note that this MARS-F modeling does not include plasma rotation nor dissipation. It is known that plasma rotation and various kinetic damping effects play an important role in the MHD stability with a resistive wall at beta above the no-wall kink limit. Here, all β_N values are lower than the calculated no-wall beta limit for the $n=3$ kink mode, $\beta_N^{\text{no-wall}, n=3} = 2.7$ and the kinetic energy of rotation is always a negligible fraction of the stored energy ($<1\%$). Also note that a direct benchmarking of the code results versus internal measurements of the plasma response is needed and in progress.

The scalings for n_i and T_i can now be recomputed from a multiple linear regression fit of the torque measurements to the torque function modified to include explicitly the beta dependence of the plasma response to the $n=3$ I-coil field, and using the previously determined exponent for ω_E ,

$$T_{\text{NRMF}} \propto \delta I_{\text{ic}}^2 \left[\left(\frac{\beta_N}{\beta_{N,0}} \right)^{1.6} + 1 \right]^2 (V_\phi - V_\phi^*) n_i^{\alpha_n} T_i^{\alpha_T} \omega_E^{-0.6}. \quad (10)$$

The new experimental scalings from this multiple linear regression fit are compared to the theoretical scalings in

TABLE II. Exponents of δI_{ic} , $(V_\phi - V_\phi^*)$, ω_E , n_i , and T_i in the theoretical expressions of the NRMF torque for the ν and $1/\nu$ collisionality regimes, and exponents (bold) from the multiple linear regression fit of the experimental measurements to the NRMF torque function modified to extract the beta dependence of the plasma response in the range $1.4 \leq \beta_N \leq 2.4$ [Eq. (8)]. The exponent for ω_E is held to the previously determined value (Table I).

	ν	Experiment [[$(\beta_N/\beta_{N,0})^{1.6} + 1$] ²	$1/\nu$
δI_{ic}	2	2	2
$V_\phi - V_\phi^*$	1	1	1
ω_E	-2	-0.6 ± 0.3	0
n_i	1	2.2 ± 0.7	-1
T_i	-0.5	1.5 ± 0.5	2.5

Table II. The results of this analysis are that, by assuming that the plasma response gives a contribution to the total perturbed magnetic field inside the plasma comparable to the external field and by separating the observed beta dependence of the plasma response from the T_i and n_i scalings, the consistency between theoretical and experimental scalings improves from the analysis using only vacuum calculations of the magnetic perturbation. Within the uncertainties, the empirical scalings for T_i , ω_E , and n_i suggest that the plasma discharges may lie in-between the asymptotic limits for the ν and $1/\nu$ regimes. Remaining disagreement could be attributed to profile effects (such as a stronger beta dependence at the minor radius chosen for the regression analysis than the dependence observed outside the plasma), or to a stronger plasma response than the MARS-F analysis indicates.

VI. SUMMARY OF RESULTS AND IMPLICATIONS FOR ITER

DIII-D experiments with application of $n=3$ magnetic fields to high beta plasmas demonstrate the existence of an offset toroidal rotation, with direction counter to the plasma current, associated with the static, nonresonant fields. When the $n=3$ field is applied to a near stationary plasma obtained by injecting small neutral beam momentum, the measured toroidal rotation of impurity ions, as well as the measured species invariant ω_E rate, and the calculated toroidal rotation of the main ions are all observed to increase in the counter direction. The rotation acceleration is large enough to cause an appreciable improvement in the global energy confinement time, consistent with $E \times B$ shear reaching critical values. The observed magnitude, direction, and radial profile of the offset rotation are consistent with neoclassical theory predictions. In DIII-D, the observed offset rotation is more than double the rotation needed for stable operation at high beta above the $n=1$ no-wall kink limit.

These experiments also provided a database of discharges with sufficient parameter variations to test the scalings of the NRMF torque. The observed strong dependence on plasma density and temperature is not consistent with neoclassical theory using vacuum calculations of the magnetic perturbation. However, the consistency between theoretical and experimental scalings improves when the plasma

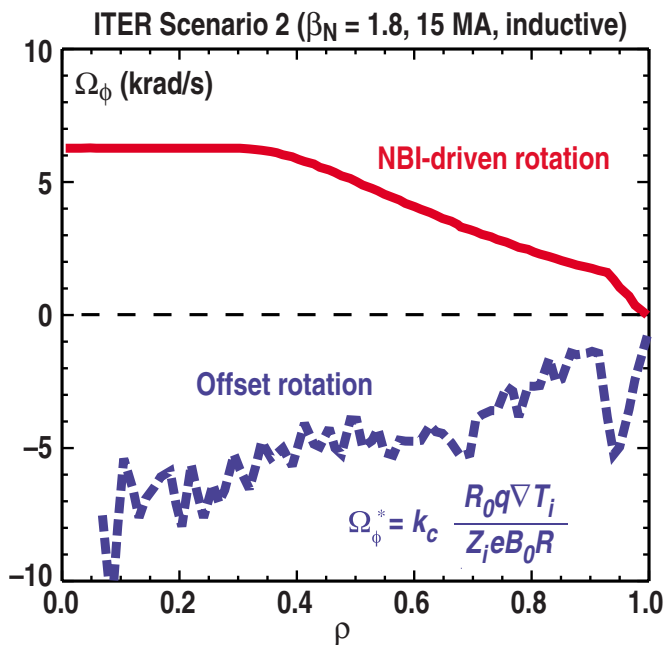


FIG. 11. (Color online) Radial profiles of the NBI-driven rotation calculated using the ASTRA code for ITER scenario 2 (Ref. 32) (red line) and the offset rotation (blue line) calculated assuming the same collisionality factor k_c measured in DIII-D and shown in Fig. 5(b).

response to the $n=3$ NRMF is assumed to be comparable to the applied field and the torque function is modified to include the measured β -dependence of the plasma response. Ideal MHD calculations of the plasma response to the $n=3$ external field support the correctness of this assumption, even at β_N significantly lower than the no-wall beta limit for the $n=3$ kink mode. In the β range of our observations, the β -dependence of the plasma response may be a key reason for the strong NRMF torque dependence on both n_i and T_i . An investigation into the radial variation of the empirical scalings, a careful benchmarking of the ideal MHD plasma response calculations, and the development of theoretical models for the collisionality regime in between the neoclassical ν and $1/\nu$ limits are all still needed for a more quantitative understanding of the NRMF torque in these experiments.

These results are particularly significant for a fusion reactor, where large externally applied nonaxisymmetric magnetic fields may be desirable for control of the pressure gradients at the edge of a high-beta H -mode plasma and suppression of ELMs. Two important implications may be summarized as follows:

- (1) The ideal MHD plasma response to the externally applied fields is likely to play a significant role in the physics of ELM suppression. It should be calculated in order to understand and predict the effect of the external fields.
- (2) The nonresonant field torque associated with the total magnetic perturbation could potentially supply the dominant rotation torque over most of the plasma minor radius, since other torque sources are expected to be weak.

For the ITER baseline mode of operation (scenario 2), the expected profiles of the NBI-driven toroidal rotation and of the neoclassical offset rotation are shown in Fig. 11. The offset rotation is about equal in magnitude to the NBI-driven rotation, but it is in the opposite direction. Note that the toroidal rotation resulting after the application of large ELM suppressing nonaxisymmetric fields is not simply given by the sum of the offset and NBI-driven rotations. The rotation in ITER will be determined by the balance of the torques acting on the plasma.

Recent calculations³³ of the expected torques from ELM suppressing fields in ITER yield damping times $\tau_{\text{dam}} = L/T_{\text{NRMF}}$ (evaluated at the NRMF turn-on time) of about 10 ms. Since the angular momentum confinement time is $\tau_L = L/T_{\text{NBI}}$ (at NRMF turn-on time) and it is generally assumed in calculations that $\tau_L \sim \tau_E$, then the ratio

$$\frac{T_{\text{NRMF}}}{T_{\text{NBI}}} = \frac{\tau_L}{\tau_{\text{dam}}}, \quad (11)$$

can be readily evaluated from the ITER scenario 2 value $\tau_E \approx 3.7$ s. The result is that the NRMF torque from ELM suppression fields in ITER scenario 2 plasmas may be up to 400 times larger than the NBI torque. In this case, the NRMF torque from turning on the ELM suppression fields would tend to bring the ITER plasma toroidal rotation from the NBI-driven profile shown in Fig. 11, through zero and close to the counter- I_p offset rotation shown in the same plot, even with co- I_p NBI. This offset rotation was calculated using the collisionality factor k_c measured in DIII-D, i.e., in plasmas that, like the ITER plasmas, are calculated to be mostly in the ν -regime of collisionality. This ITER offset rotation, which is about 0.4% of the Alfvén frequency, may be sufficient to benefit confinement and stability. However, issues related to the transition in rotation from NBI driven to NRMF-driven, particularly during the crossing of zero rotation, will need further investigation.

ACKNOWLEDGMENTS

This work was supported by the U.S. Department of Energy under DE-FC02-04ER54698, DE-AC02-76CH03073, and DE-FG02-89ER53297.

The authors wish to thank J.D. Callen for having provided the impetus to explore experimentally the offset rotation.

¹K. H. Burrell, *Science* **281**, 1816 (1998).

²R. J. Buttery, R. J. La Haye, P. Gohil, G. L. Jackson, H. Reimerdes, and E. J. Strait, and the DIII-D Team, *Phys. Plasmas* **15**, 056115 (2008).

³A. M. Garofalo, G. L. Jackson, R. J. La Haye, M. Okabayashi, H. Reimerdes, E. J. Strait, J. R. Ferron, R. J. Groebner, Y. In, M. J. Lanctot, G. Matsunaga, G. A. Navratil, W. M. Solomon, H. Takahashi, M. Takechi, A. D. Turnbull, and the DIII-D Team, *Nucl. Fusion* **47**, 1121 (2007).

⁴J. E. Rice, M. Greenwald, I. H. Hutchinson, E. S. Marmor, Y. Takase, S. M. Wolfe, and F. Bombarda, *Nucl. Fusion* **38**, 75 (1998).

⁵J. S. deGrassie, J. E. Rice, K. H. Burrell, R. J. Groebner, and W. M. Solomon, *Phys. Plasmas* **14**, 056115 (2007).

⁶Z. Chang and J. D. Callen, *Nucl. Fusion* **30**, 219 (1990).

⁷R. Fitzpatrick and T. C. Hender, *Phys. Fluids B* **3**, 644 (1991).

⁸R. Fitzpatrick, *Phys. Plasmas* **5**, 3325 (1998).

⁹T. H. Stix, *The Theory of Plasma Waves* (McGraw-Hill, New York, 1962), p. 207.

- ¹⁰R. J. La Haye, S. Gunter, D. A. Humphreys, J. Lohr, T. C. Luce, M. E. Maraschek, C. C. Petty, R. Prater, J. T. Scoville, and E. J. Strait, *Phys. Plasmas* **9**, 2051 (2002).
- ¹¹H. Reimerdes, M. S. Chu, A. M. Garofalo, G. L. Jackson, T. H. Jensen, R. J. La Haye, G. A. Navratil, M. Okabayashi, J. T. Scoville, and E. J. Strait, 30th EPS Conference on Controlled Fusion and Plasma Physics (St. Petersburg, Russia, 2003), Europhysics Conference Abstracts, Vol. 27A, P-4.45.
- ¹²W. Zhu, S. A. Sabbagh, R. E. Bell, J. M. Bialek, M. G. Bell, B. P. LeBlanc, S. M. Kaye, F. M. Levinton, J. E. Menard, K. C. Shaing, A. C. Sontag, and H. Yuh, *Phys. Rev. Lett.* **96**, 225002 (2006).
- ¹³K. C. Shaing, *Phys. Fluids* **29**, 521 (1986).
- ¹⁴K. C. Shaing, *Phys. Plasmas* **10**, 1443 (2003).
- ¹⁵T. E. Evans, R. A. Moyer, P. R. Thomas, J. G. Watkins, T. H. Osborne, J. A. Boedo, E. J. Doyle, M. E. Fenstermacher, K. H. Finken, R. J. Groebner, M. Groth, J. H. Harris, R. J. La Haye, C. J. Lasnier, S. Maszaki, N. Ohyaabu, D. G. Pretty, T. L. Rhodes, H. Reimerdes, D. L. Rudakov, M. J. Schaffer, G. Wang, and L. Zeng, *Phys. Rev. Lett.* **92**, 235003 (2004).
- ¹⁶A. Cole, C. Hegna, and J. Callen, *Phys. Rev. Lett.* **99**, 065001 (2007).
- ¹⁷A. M. Garofalo, K. H. Burrell, J. C. DeBoo, J. S. deGrassie, G. L. Jackson, M. Lanctot, H. Reimerdes, M. J. Schaffer, W. M. Solomon, and E. J. Strait, *Phys. Rev. Lett.* **101**, 195005 (2008).
- ¹⁸G. L. Jackson, P. M. Anderson, J. Bialek, W. P. Cary, G. L. Campbell, A. M. Garofalo, R. Hatcher, A. G. Kellman, R. J. La Haye, A. Nagy, G. A. Navratil, M. Okabayashi, C. J. Pawley, H. Reimerdes, J. T. Scoville, E. J. Strait, and D. D. Szymanski, *Europhys. Conf. Abstr.* **27A**, P-4.47 (2003).
- ¹⁹W. A. Houlberg, K. C. Shaing, S. P. Hirshman, and M. C. Zarnstorff, *Phys. Plasmas* **4**, 3230 (1997).
- ²⁰W. M. Solomon, K. H. Burrell, R. Andre, L. R. Baylor, R. Budny, P. Gohil, R. J. Groebner, C. T. Holcomb, W. A. Houlberg, and M. R. Wade, *Phys. Plasmas* **13**, 056116 (2006).
- ²¹J. S. deGrassie, J. E. Rice, K. H. Burrell, R. J. Groebner, and W. M. Solomon, *Phys. Plasmas* **14**, 056115 (2007).
- ²²K. C. Shaing and E. C. Crume, Jr., *Phys. Rev. Lett.* **63**, 2369 (1989).
- ²³H. Biglari, P. H. Diamond, and P. W. Terry, *Phys. Fluids B* **2**, 1 (1990).
- ²⁴T. S. Hahm and K. H. Burrell, *Phys. Plasmas* **2**, 1648 (1995).
- ²⁵G. M. Staebler, J. E. Kinsey, and R. E. Waltz, *Phys. Plasmas* **12**, 102508 (2005).
- ²⁶H. Reimerdes, A. M. Garofalo, M. Okabayashi, E. J. Strait, R. Betti, M. S. Chu, B. Hu, Y. In, G. L. Jackson, R. J. La Haye, M. J. Lanctot, Y. Q. Liu, G. A. Navratil, W. M. Solomon, H. Takahashi, R. J. Groebner, and the DIII-D Team, *Plasma Phys. Controlled Fusion* **49**, B349 (2007).
- ²⁷L. M. Kovrizhnykh, *Nucl. Fusion* **24**, 851 (1984).
- ²⁸A. Cole, C. Hegna, and J. Callen, *Phys. Plasmas* **15**, 056102 (2008).
- ²⁹W. M. Solomon, K. H. Burrell, A. M. Garofalo, A. J. Cole, R. V. Budny, J. S. deGrassie, W. W. Heidbrink, G. L. Jackson, M. J. Lanctot, R. Nazikian, H. Reimerdes, E. J. Strait, and M. A. Van Zeeland, "Advances in understanding the generation and evolution of the toroidal rotation profile on DIII-D," *Nucl. Fusion*. (submitted).
- ³⁰R. Hawryluk, in *Phys. Plasmas Close to Thermonuclear Conditions*, edited by B. Coppi, G. G. Leotta, D. Pfirsch, R. Pozzoli, and E. Sindoni (CEC, Brussels, 1980), Vol. 1, pp. 19–46.
- ³¹Y. Q. Liu, A. Bondeson, C. M. Fransson, B. Lennartson, and C. Breitholtz, *Phys. Plasmas* **7**, 3681 (2000).
- ³²A. R. Polevoi, M. Shimada, M. Sugihara, Yu. L. Igitkhanov, V. S. Mukhovatov, A. S. Kukushkin, S. Yu. Medvedev, A. V. Zvonkov, and A. A. Ivanov, *Nucl. Fusion* **45**, 1451 (2005).
- ³³M. Becoulet, G. Huysmans, X. Garbet, E. Nardon, M. Schaffer, A. Garofalo, K. Shaing, A. Cole, J.-K. Park, and P. Cahyna, *Proceedings of the 22nd IAEA Fusion Energy Conference*, Geneva, Switzerland (IAEA, Vienna, 2008), Paper No. TH/2–1ra.